Automated Quantitative Assessment of Perifollicular Vascularization Using Power Doppler Ultrasound Images

BORIS CIGALE, SMILJAN ŠINJUR, DAMJAN ZAZULA
Faculty of Electrical Engineering and Computer Science
University of Maribor
Smetanova ulica 17, Maribor
SLOVENIA
boris.cigale@uni-mb.si http://storm.uni-mb.si

Abstract: - In this paper a prototype of automated quantitative assessment of perifollicular vascularisation is described. Assessment of perifollicular vascularisation is important in the research, perfomed by medical team at the Teaching Hospital of Maribor, if the application of hormonal therapy after follicle puncture in natural cycles is really always needed. The proposed algorithm works with 3D power Doppler ultrasound images and consists of several steps. At the first step the position and shape of the dominant follicle is determined. The procedure based on the continuous wavelet transform is utilized. Then vessels contained in 5 mm thick layer around the follicle are categorized according to their diameter. The vessel thickness at certain point is defined as diameter of the largest sphere which includes points and fits entirely inside vessels. The results are statistically evaluated by the histograms of vessel diameters. To improve the visual results the vessel reconstruction, based on minimal spanning trees, is done at the end.

Key-Words: - 3D ultrasound image segmentation, vessel thickness assessment, vessel reconstruction

1 Introduction

Prior to ovulation, the vascular layer of the follicle plays a significant role in ensuring the conditions for normal oocyte development, and after ovulation in the development of the gland (corpus luteum), which is important in creating the conditions required for conception. In assisted reproduction technology procedures (ART), the contents of the ovarian follicle are aspirated, whereby some granulosa cells are removed and the vessels developing around the follicle are damaged (perifollicular vascularization). This is particularly important in ART in natural cycles, when only one follicle is present and its function is important for the outcome of the therapeutic procedure. In the last 20 years, the literature does not report what kind of vascular damage occurs during follicle puncture and how it affects corpus luteum development. Assuming that the functional disturbance does occur, all women receive medication to support the corpus luteum activity after the ART procedure. By analyzing the characteristics of vascularization in the corpus luteum, which develops after ART in a natural cycle, it would be possible to objectivize its function as well as any vascular damage caused by the puncture. This would guide the medical personnel to objectively appraise the need for application of hormonal therapy after follicle puncture in natural cycles. Also, it would mean an option for objective comparison between the corpora lutea characteristics developed in spontaneous, natural ovulation and those developed after the ART puncture of the dominant follicle in a natural cycle.

In this paper, we propose computer-based techniques helping the medical experts to accomplish this study. Our solution is based on 3D colour Doppler ultrasound (US) images. Colour Doppler US investigation is a safe, fast and noninvasive method used to measure the blood flow rate. The 3D colour US images can serve the estimation of the volume and the position of individual vessels.

The algorithms we developed so far detect the position, volume and diameter of the vessels surrounding the ovarian follicles. Using procedures based on wavelet transform, we first find the position of the follicle in every image, as it is described in Section 2. After the position of the follicle is known, we can determine the area to be searched for the vessels. The vessels are categorized according to their diameter and the results are statistically evaluated by the histograms of vessel diameters and spatial vessel distribution, as explained in Section 3. In Section 4, we describe our novel algorithm for vessel reconstruction based on the minimal spanning trees. In Section 5 the results are summarized. This is followed by conclusions.

2 Detection of follicles

Ovarian follicles are spherical-like fluid-filled structures. Their growth stops at 8 to 10 mm on average, only the dominant follicle can reach as much as 17-25 mm in

diameter [3]. A follicle in 3D US images is seen as a spherical homogenous region whose average greyness is darker than the surroundings. However, other objects with similar characteristics exist in the image (e.g. veins). This aggravates the segmentation of follicles, which means the initial step for automated quantitative assessment of perifollicular vascularization. Therefore, we paid particular attention to finding the position and the shape of follicles using ordinary 3D US imaging, i.e. US volumes. Length of one voxel is around 0.2 mm in such images, thus expected diameter of the fully grown dominant follicle is around 85 voxels or more. The example of 3D ultrasound volume is depicted in Fig. 1.

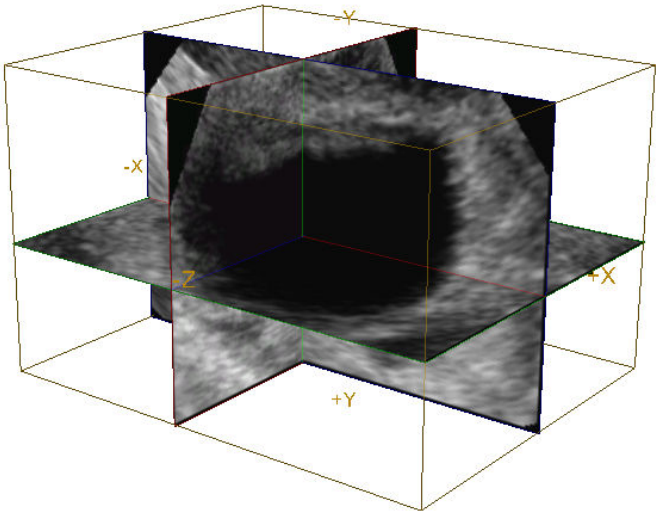

Figure 1: 3D view on the ultrasound volume

Many algorithms exist for the segmentation of ultrasound images [1-6]. Most of the algorithms enable automated or semi-automated segmentation of 2D ovarian ultrasound images [1-3], but only a few of them [4-6] can be extended to 3D images that provide more information. We implemented a variation of the method [6] based on continuous wavelet transform.

The detection of follicles consists of two consecutive steps; firstly, the follicle centroid is determined using continuous wavelet transform and, secondly, the shape of previously detected follicle is outlined.

2.1 Detection of the follicle centroid

Since follicles have spherical shape in 3D, they are very suitable for the detection by the 3D Mexican hat (MH) wavelet (depicted in Fig. 2), which is isotropic and, therefore, has spherical shape. In 3D, point (x, y, z) in MH is defined as:

$$\psi(x,y,z) = (3 - x^2 - y^2 - z^2)\; e^{-(x^2+y^2+z^2)/2}. \qquad (1)$$

MH can be scaled by factor a which is equal for all dimensions and can also be translated, where a shift is described by vector $b = (b_x, b_y, b_z)$. By using scale a and shift b, Eq. (1) becomes:

$$\psi_{a,b}(x,y,z) = \frac{1}{a^{3/2}}\psi\left(\frac{x-b_x}{a}, \frac{y-b_y}{a}, \frac{z-b_z}{a}\right). \qquad (2)$$

Continuous wavelet transform of function $f(x,y,z)$ is defined as:

$$W_f(a,b) = \int_{-\infty}^{\infty}\int_{-\infty}^{\infty}\int_{-\infty}^{\infty} \psi_{a,b}(x,y,z)\, f^*(x,y,z)\, dx\, dy\, dz. \qquad (3)$$

where $f^*(x,y,z)$ denotes the complex conjugate of $f(x,y,z)$.

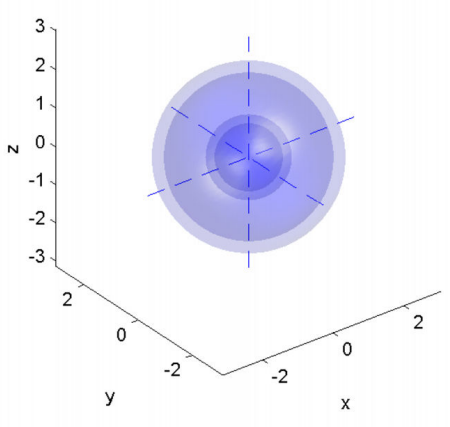

Figure 2: Mexican hat in 3D

When modelling the follicle as a sphere S with greyness 1 and the surrounding tissue with greyness 0, it can be proved [6] that its wavelet transform exhibits a local extreme in the follicle's centroid. We denote the radius of the sphere with C. For a's that squeeze the wavelet inside the follicle, a local minimum appears at the follicle's centroid position (Fig. 3 and 4). When scale a is much smaller than follicle (when scales $a<(C-0.5)/3.5$), then values of the wavelet transform in the centroid position and its neighbourhood limits toward 0 in the ideal theoretical case. On real data even values smaller than 0 can be obtained in the centroid. The experiments showed that the results of the wavelet transform are very sensitive to the noise at such scales. We showed in [6] that the most suitable scales for the detection of the follicle centre is when scale a is in the interval:

$$\frac{C-0.5}{3.5} < a < \frac{C}{2}. \qquad (4)$$

The wavelet transform at such scales still has the local minimum in the follicle's centroid, but the result is not so sensitive to the noise anymore. The extreme in the centroid corresponds to a maximum when the scale *a* expands the MH wavelet outside the follicle's borders (Fig. 5).

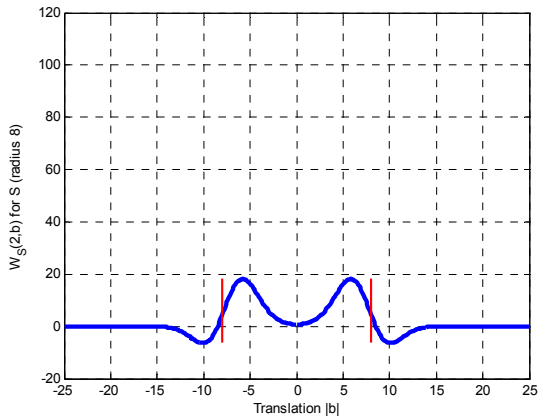

Figure 3: Wavelet transform of the follicle model with radius 8 at scale 2.

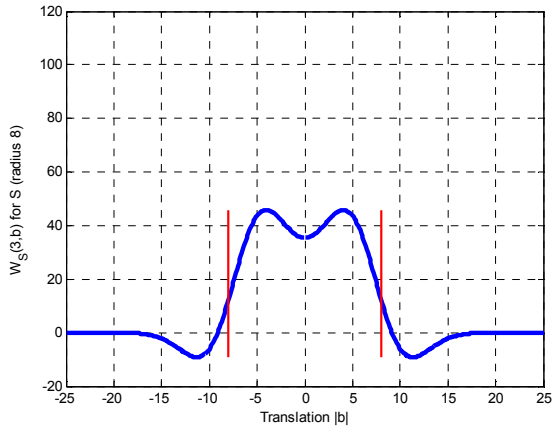

Figure 4: Wavelet transform of the follicle model with radius 8 at scale 3.

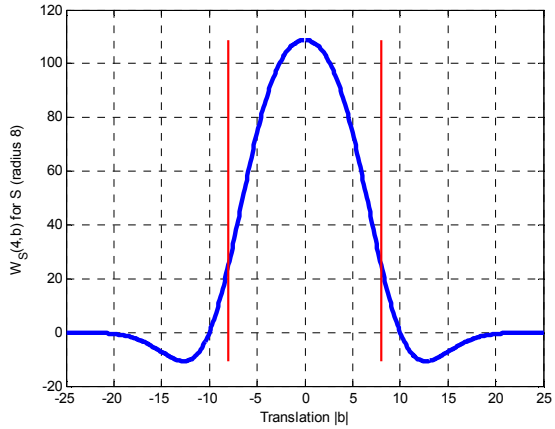

Figure 5: Wavelet transform of the follicle model with radius 8 at scale 4.

Our algorithm for the detection of centroids in dominant follicles is based on the tracking of local extremes through the different scales. Local maximums are not taken into account because they are very error prone due to the noise which is severely present in real follicle recordings, where follicle's surrounding is not monotonic as assumed in the theoretical model.

The procedure begins at the highest scale a_b, in which we try to detect the largest follicles, and ends at scale a_e, where we try to detect the smallest ones. The coordinates of all local minimums in a US volume at scale a_t are stored into a dataset C_t. Each minimum in C_t is tested for adequacy by checking the voxel in original image at the same coordinates. If the greyness of the voxel exceeds a preselected threshold T, the minimum is dropped from the set C_t. Then, for each coordinate k_i^t in C_t the nearest coordinate k_j^{t+1} in the set C_{t+1} is found. The coordinate k_j^{t+1} and scale $t+1$ are added to the set of local minimums, M, if Euclidian distance $|k_i^t - k_j^{t+1}| < H$, where H stands for a maximum allowed distance (usually 5). In general, the minimum which can be traced successively through three different scales is a good candidate for a follicle's centroid position. However, when dealing with dominant follicles, as in the described application, we can safely assume the follicle is the greatest object in the US volume. Hence, the sequence of minimums, which starts at the highest scale an can be traced through three different scales, is declared as follicle centroid.

Pseudocode of the algorithm is depicted in Fig. 6.

```
function DetectionOfDominantCentroid(volume, a_b,a_e)
 for a_t = a_b to a_e step -1
  W=calculateCWT(volume, a_t)
  Ct=localMinimums(W)
  foreach coordinate k_i^t in Ct
   if volume(k_i^t)> T
    drop k_i^t from Ct
   else
    k_j^{t+1}=findNearest(k_i^t, C_{t+1})
    if euclidianDistance (k_i^t, k_j^{t+1}) < H
     M = addToSet(M,a_t,k_i^t, k_j^{t+1})
    else
     M = addToSet(M,a_t,k_i^t, 0)
    end if
    if M(end,4)==3  // if the centroid can be traced
     return k_i^t        // through 3 scales, return it
    end if
   end if
  next c
 next a
 return DominantCentroidNotDetected
end

function cm=findNearest(k,C)
 minD=maxValue;
 foreach coordinate c in C
  if euclidianDistance(c,k)<minD
```

```
    cm=c
   end if
  next c
end

function M=addToSet(M,a,s,f)
// function adds new connection to the set M.
// M is 2D table, first column represents scale a,
// second columen the coordinates of the centroid
// s and third column the row in M where the coordinates
// of centroid at scale a-1 are stored
// in fourth column we track the number od scales at which
// the center was detected
  indf=find(M(:,1)==a-1 & M(:,1)==f)
  M(end+1,:)=[a s indf M(indf,4)+1] // append new row to M
end
```

Figure 6: Algorithm for detection of the follicle centroid

2.2 Outlining the follicle

After the follicle centroid is detected the follicle shape must be outlined. Our method for outlining was again inspired by the study of wavelet behavior. It can be seen from Figs. 3, 4 that if we travel from point b=0 in either direction, we eventually hit the local maximum, when scale a decreases below the follicle's size. It has been proved [6] that this maximum is roughly positioned at the point b=r-a, where r means follicle's radius. The distance of the follicle's edge from the centroid can be thus calculated as:

$$r = b + a\,. \tag{4}$$

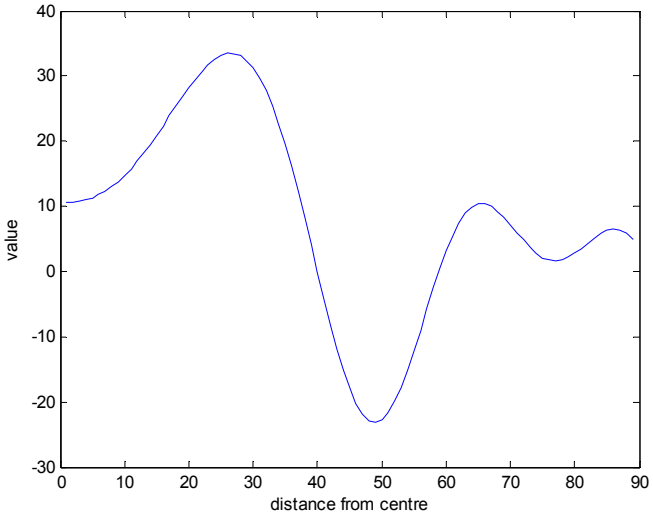

Figure 7: Transformed values sampled along ray on real data

This phenomenon provides us with a tool for the calculation of the follicle border points. We calculate the border points from the wavelet transform in scale a in which the centroid was found. We generate 132 radial rays in homogeneous orientation distribution [7], casted outwards from each detected centroid. The radial rays casted from the centroid are not new approach to the shape outlining. The similar approach in the filed of the ovarian 3D ultrasound image segmentation was published in [4]. The transform values are sampled along the rays at integer distances n, beginning from the centroid's coordinates k_j^{t+1} in the direction of spherical angles θ and φ. Thus, $r_{\theta,\varphi}(n)$ designates the weighted-average greyness of voxels in a US sub-volume, defined by the wavelet scale, at radius n in the direction θ and φ. In such a way, a graph similar to one depicted in Fig. 7 is obtained, and the distance of the follicle border points in given direction can be calculated.

All border voxels are organized into triangular mesh which is then smoothed by mesh smoothing method [8]. The result of the segmentation is depicted in Fig. 8 and the pseudocode of the algorithm is depicted in Fig. 9.

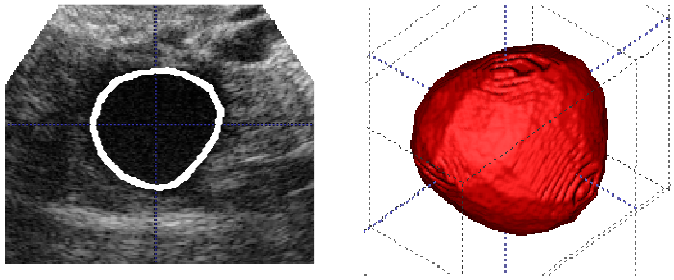

(a) (b)

Figure 8: Annotated position of follicle in one slice (a), reconstructed 3D model of follicle (b).

```
function FollicleOutlining(volume, a_b,k)
  W=calculateCWT(volume, a_t)
  AngThPh=getAngles132EqualyDistributedSphericalPnts()
  foreach angle theta,phi in AngThPh
    line=sampleLine(volume, k, theta, phi)
    b=findPositionOfFirstMinimum(line)
    r = b + a_b
    x_b= r*cos(theta)*sin(phi)
    y_b= r*sin(theta)*sin(phi)
    z_b= r*cos(phi)
    borderPoints(theta,phi)=[ x_b, y_b, z_b]
  next theta,phi
end
```

Figure 9: Algorithm for detection of the follicle outlining

3 Quantitative Assesment of Perifollicular Vascularization

Aiming at the final detection of perifullicular vascularisation, we deploy US imaging of two modalities. Ordinary 3D US images are used for the dominant follicle detection, while power Doppler images show the areas with blood flow, i.e. blood vessels the observed dominant follicle.

Only the vessels that surround the follicle in a 5 mm thick layer are taken into consideration, as explained in the sequel. Prior that step the Doppler image is binarised by threshold function to reduce noise.

We first assess the thickness of blood vessels. They provide us with enough information to calculate a simple quantitative measure of perifollicular vascularization. Centroids of the so called maximal balls [9], which are the side result of the vessel thickness assessment, are further used in the vessel reconstruction algorithm.

Denote a set of voxels positioned in vessels, by F and a voxel i in this set by p_i. The 3×3×3 neighbourhood of voxel p_i is denoted by $N(p_i)$. $N_{26}(p_i)=N(p_i)- p_i$ denotes the set of 26 voxels adjacent to p_i.

Figure 10: Typical input to the vessel thickness assessment procedure. In the centre is annotated position of follicle, the 5 mm thick layer around follicle is also annotated. The position of vessels surrounding the follicle is shown.

3.1 Vessel thickness assessment

We are interested in thickness of vessels surrounding the follicle. In [10], authors define the local thickness at given voxel p_i inside a structure as the diameter of the largest sphere which includes the voxel and which fits entirely the structure. Brute force search for such spheres could be very time demanding, therefore more refined approach were developed. A solution comes in the form of maximal balls, i.e. spheres, lying entirely inside the observed structure and being disjunctive with all other spheres. Such maximal balls form a set of candidate spheres.

Each voxel from the structure is then tested for inclusion into one of maximal balls. The sphere with maximum radius is chosen from all the maximal spheres containing the tested voxel.

3.1.1 Centroids of maximal balls

To each voxel p_i in F we can append a sphere (usually referred to as a ball) s_i with its centroid in p_i and radius r_i representing the Euclidean distance from the voxel p_i to the nearest voxel lying outside of vessels. Therefore, all voxels positioned inside the ball belong to the vessels. Maximal balls, comprising a subset of balls, are those that are not completely contained in any other ball. The centroids of maximal balls (CMB) are usually positioned in the centroids of objects.

Many algorithms exist for the calculation of the CMB. We used the algorithm published in [9]. This algorithm uses Chamfer distance instead of the Euclidean one. This speeds up the algorithm since the calculation of the Euclidean distance is much more time consuming.

Chamfer distance is the approximation of Euclidian distance, where the distance from voxel p_i to the nearest voxel positioned outside of the vessels is computed with the help of neighbouring points [11]. The distance is defined recursively as:

$$d(p_i)=\begin{cases}\min\{d(p_j)+D(p_i,p_j)\} & p_i\in F\\ 0 & p_i\in \overline{F}\end{cases} \quad (4)$$

where $D(p,q)$ is an integer approximation to the Euclidian distance between pairs of adjacent points

$$D(p_i,p_j)=\begin{cases}3, & \|p_i-p_j\|^2=1\\ 4, & \|p_i-p_j\|^2=2\\ 5, & \|p_i-p_j\|^2=3\end{cases} \quad (5)$$

It has been shown in [9] that centroids c_i of maximal balls satisfy

$$d(c_i)\neq d(p_j)-D(c_i,p_j),\forall p_j\in N_{26}(c_i) \quad (6)$$

3.2 Calculation of statistics

In order to assess perifollicular vascularization statistically we introduced two histograms. The histograms are important for medical diagnosing and treatment.

The first histogram shows the number of voxels belonging to blood vessels with the certain thickness. This gives us a general idea about the structure of the vessels that surround the dominant follicle (i.e. the quantity of thin vessels versus the thick ones). The histogram is obtained from the vessel thickness assessment and example is depicted in Fig. 11.

Another histogram shows the spatial distribution of vessels around the follicle. It gives an impression whether the distribution is uniform around the follicle or concentrations appear in parts of the follicle. The histogram is constructed based on 117 equally sized sectors surrounding the follicle's centroid. For each vessel thickness, the portion of sectors containing such vessels is depicted in Fig. 11.

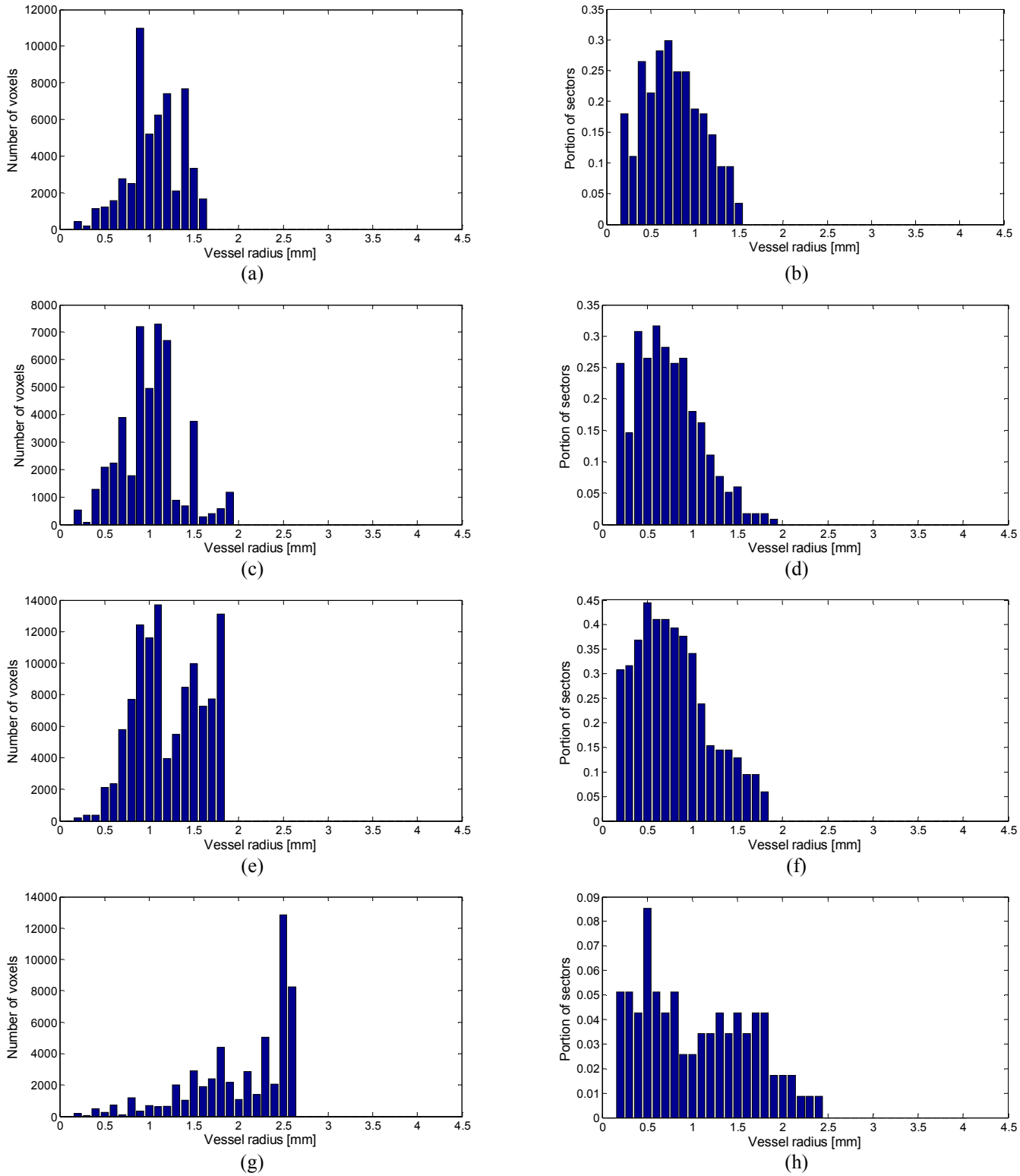

Figure 11: The number of voxels belonging to blood vessels with the certain thickness for images 1 (a), 2 (c), 3 (e) and 4 (g). The portion of sectors containing the vessels with certain radius for images 1 (b), 2 (d), 3 (f) and 4 (h). Images 1 and 2 belong to the same patient.

4 Vessel reconstruction

Power Doppler images show the areas with blood flow, however usually not all vessels are equally visible. The most visible are wide vessels with high pressure. Thus most of the arteries are discovered, but not all veins and capillaries.

Another problem is that vessel is sometimes not perceived entirely, but only on regions where the pressure is highest, for example where vessel splits into two or more vessels.

Therefore a method which will reconstruct the vessels from power Doppler images is desired. Such reconstruction will not affect much the statistical results (i.e. the portion of sectors containing the vessels) however it will ease the interpretation of the results to the patients.

4.1 Algorithm

Our novel vessel reconstruction algorithm is based on minimal spanning trees [12]. It consists of several steps as shown in Fig. 12. The input to the algorithm is binarized power Doppler image.

```
function VesselReconstruction(volume, radius)
  // compute Chamfer distances on voxels
  chD = chamferDistance(volume);
  // find only local maximums since we are interested only on
  // vessel centres
  LMVertices = findLocalMaximums(chD, radius);
  // compute Euclidian distances between all local maximums
  distance = computeDistances(chD);
  // Prim's algorithm to compute minimum spanning tree of
  // local maximums and their mutual distances
  minTree = minimumSpanningTree(LMVertices, distance);
  // Bresenham rasterization on nodes of a given minimum
  // spanning tree
  oVolume = computeBresenham(minTree, chD);
  // reconstruction of vessels in new volume
  sVolume = createSphereVolume(oVolume, chD);
end

function oVolume = computeBresenham(minTree, chD)
  // minTree is a set of connected nodes – two vertices in
  // minimum spanning tree
  foreach node in minTree
    // Euclidian distance between node vertices
    d = distance(node);
    // size of vessel in first vertex
    s0 = getVesselSize(node[0]);
    // size of vessel in second vertex
    s1 = getVesselSize(node[1]);
    // compute raster voxels according to Bresenham
    // algorithm
    b = Bresenham(node);
    foreach rasterVoxel in b
      // compute Euclidian distance between starting vertex and
      // rasterVoxel
      d1 = distance(node[0], rasterVoxel);
      // compute vessel size in rasterVoxel
      oVolume[rasterVoxel[X][Y][Z] = d1/d * (abs(s1-s2))+s1;
    next rasterVoxel
  next node
end
```

Figure 12: Algorithm for vessel reconstruction

At the beginning we calculate the Chamfer distances for voxels representing the vessels as described in 3.1.1.

In second stage all local maximums are identified in Chamfer distance matrix. Local maximums define the centres of vessels. To reduce the noise (i.e. falsely indentified centres) all returned maximums are required to be the global ones in predefined radius.

Matrix of local maximums is sparse matrix with only a few of the elements – vessel centers. Since we know the radius for each element in sparse matrix the initial volume could be reconstructed. Cardio vascular system of a human body is very similar to set of trees, especially if arteries and veins are observed separately. As mentioned before, Doppler image perceives mostly arteries and some of the larger veins. To create a model of cardio vascular system around the follicle minimum spanning tree from identified vessels centres is created [13]. Since matrix of local maximums is sparse matrix, only small amount of voxels has to be processed. Algorithm used in this stage is so called Prim's algorithm which gives optimal result in short amount of time [14]. Searching criteria to compute minimum spanning tree is Euclidian distance between local maximums voxels in volume.

Result of Prim's algorithm is a set of connected pairs of vertices, where connection simulates the vessel path. All joined pairs define 3-dimensional tree. In the resulting set only edges - nodes of a tree are defined and additional rasterization has to be performed. For each resulting pair of vertices 3D version of Bresenham rasterization [15], [16] is calculated. Special care is taken thereby since the vertices of the pair usually do not belong to the vessels with the same radius. For all rasterized vertices between all nodes linear approximation of vessel size is computed, according to the distance between raster and starting vertex and size of vertices of a node. Resulting volume with edge and raster vertices represent the centres of reconstructed vessels. For each vertex a radius was calculated in previous step. The sphere's radius is equal to the vertex's Chamfer distance and the centre of such a sphere lies on vertex. All spheres are merged into new volume - volume of reconstructed vessels.

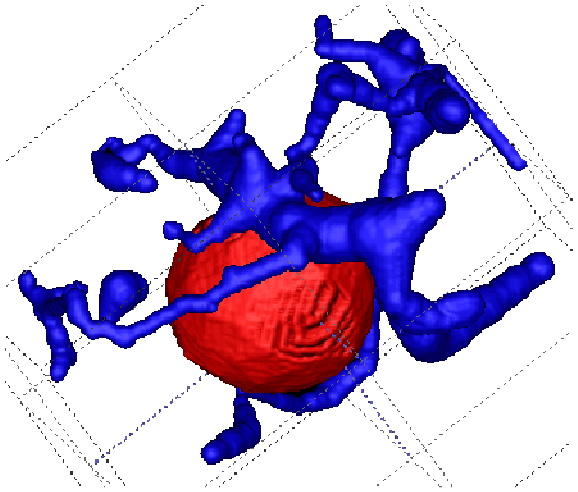

Figure 13: Follicle and reconstructed vessels

4.2 Analysis

It was shown that cardio vascular reconstruction around and inside follicle is possible from a Doppler image. However more extensive testing should be performed. The problem is that we did not know the ground truth, i.e. the actual vessel state, but medical personnel confirmed that reconstructed state is very close to the state as it should be. One example is depicted in Fig. 6 which shows the volume at early stage, where only one artery encircles the follicle.

Nodes of our reconstructed tree indicate the separation of a vessel and lists of our tree points out to the connections of the artery with capillaries.

Time complexity for described vessel reconstruction is $O(n^2)$, where n is number of local maximums vertices. Measurements show that for a given Doppler volume number of local maximums vertices is much smaller according to the volume vertices. Most time consuming step of the algorithm is computing Euclidian distances between local maximums. In future, this step will be reduced, since distances of all pair do not have to be computed. To achieve similar results only distances between vertices in some local region has to be computed.

5 Results

The algorithm was tested on the four images provided by the Teaching Hospital of Maribor and the results were also visually evaluated by medical personnel.

The position of the dominant follicle was automatically detected on all images. The threshold for power Doppler images was set manually for each image.

The quantitative assesment of perifollicular vascularization for all four images is depicted in Fig. 11. Especially interested are the results for images 1 and 2, since they belong to the same patient. It can be seen, that the shape of the histogram is similar, however not equal. This can be explained by the nature of power Doppler imaging where the vessels are not always equally visible.

The results of the vessels reconstruction algorithm is depicted in Figs. 13 and 14. Again the special attention should be paid to images 1 and 2 in Fig. 14, since they belong to the same patient. It can be easily seen that the reconstructed vessels are similar.

6 Conclusions

The first prototype of the automatic procedure for quantitative assessment of perifollicular vascularisation is described in this paper. The procedure work perfectly on test images provided to us although more extensive testing must be perform especially with the trained medical personnel.

Our future work will focus on building the nicer user interface, designed specially for the use of medical personnel. We will also add additional statistics if the medical research will show that it is required.

Due to the nature of Doppler ultrasound its resolution is smaller than the resolution of normal ultrasound and usually not all vessels are equally visible. We believe that power Doppler result could be improved by combining the information of several ultrasound images obtained consecutively in the same examinations. This could be done using rigid image registration, where the follicles in the normal US would be registered firstly. With obtained transformation the power Doppler US could be also registered. For the registration the algorithm [17] could be used.

We will also try to improve vessel reconstruction part of our procedure. By doing so it will be possible to use non-rigid registration of medical images and thus we will be able to visualize the vessel development on daily basis which will undoubtedly help the medical expert to understand the behaviour of perifollicular vascularisation more thoroughly.

Acknowledgment

We would like to thank Prof. Veljko Vlaisavljević from the Teaching Hospital of Maribor for provided images and valuable help.

This work was supported by Slovenian Research Agency (ARRS) in the project J3-0674.

References:

[1] B. Cigale, D. Zazula, Segmentation of Ovarian Ultrasound Images Using Cellular Neural Networks, *International Journal of Pattern Recognition and Artificial Intelligence*, Vol. 18, No. 4, 2004, pp. 563-581.

[2] A. Krivanek, M. Sonka, Ovarian Ultrasound Image Analysis: Follicle Segmentation, *IEEE Transaction on medical imaging*, Vol. 17, No. 6, 1998, pp. 935-944.

[3] B. Potočnik, D. Zazula, Automated analysis of a sequence of ovarian ultrasound images. Part I, Segmentation of single 2D images, *Image and Vision Computing*, Vol. 20, No. 3, 2002, pp. 217-225.

[4] B.M.H. Romeny, B. Tirtulaer, S. Kalitzin, G. Scheffer, F. Broekmans, J. Staal, E. Velde, Computer assisted human follicle analysis for fertility prospects with 3D ultrasound, *Lecture notes in computer science,* Vol. 1613, 1999, pp. 56-69.

[5] M.J. Gooding, S. Kennedy, J.A. Noble, Volume segmentation and reconstruction from freehand three-dimensional ultrasound data with application to ovarian follicle measurement, *Ultrasound in medicine and biology*, Vol. 34, No. 2, 2008, pp. 183-195.

[6] B. Cigale, *A Multiscale Approach to Detection and Growth Assessment of Structures in 3D Ultrasound Volumes*, PhD Thesis, Faculty of Electrical engineering and Computer Science, Maribor, 2007.

[7] N. J. A. Sloane, R. H. Hardin, W. D. Smith, Tables of Spherical Codes, *published electronically at www.research.att.com/~njas/packings/*, 15.1.2010.

[8] A. Belyaev, Y. Othake, A comparison of mesh smoothing methods, *Israel-Korea Bi-National Conference on Geometric Modeling and Computer Graphics*, Tel Aviv University, 2003, pp. 83-87.

[9] C. Pudney, Distance-Ordered Homotopic Thinning: A Skeletonization Algorithm for 3D Digital Images, *Computer Vision and Image Understanding*, Vol. 72, No. 3, 1998, pp. 404-413.

[10] T. Hildebrand, P. Rüegsegger, A new method for the model-independent assessment of thickness in three-dimensional images, *Journal of Microscopy*, Vol. 185, No. 1, 1997, pp. 67-75.

[11] M. W. Jones, J. A. Baerentzen, M. Sramek, 3D Distance Fields: A Survey of Techniques and Applications, *IEEE Transactions on Visualization and Computer Graphics*, Vol. 12, No. 4, 2006, pp. 581-599.

[12] E. Milková, Constructing knowledge in graph theory and combinatorial optimization, *WSEAS Transactions on Mathematics*, Vol. 8, No. 8, 2009, pp. 424-434.

[13] T. H. Cormen, C. E. Leiserson, R. L. Rivest, C. Stein, *Introduction to Algorithms, Second Edition*, MIT Press and McGraw-Hill, 2001.

[14] D. R. Karger, P. N. Klein, R. E. Tarjan, A randomized linear-time algorithm to find minimum spanning trees, *Journal of the ACM*, Vol. 42, No. 2, 1995, pp. 321-328.

[15] J. E. Bresenham, Algorithm for computer control of a digital plotter, *IBM Systems Journal*, Vol. 4, No.1, 1965, pp. 25–30.

[16] L. I. Dimitrov, M. Sramek, Using 3D-Bresenham for Resampling Structured Grids, *Proceedings of the 3D Data Processing, Visualization, and Transmission*, 2nd International Symposium, 2004, pp. 926-930.

[17] S. Šprager, B. Cigale, D. Zazula, Estimation of Growth of Ovarian Follicles Using Rigid and Elastic Ultrasound Image Registration, to appear in *proceedings of BIOSIGNALS 2010*, Spain, 2010.

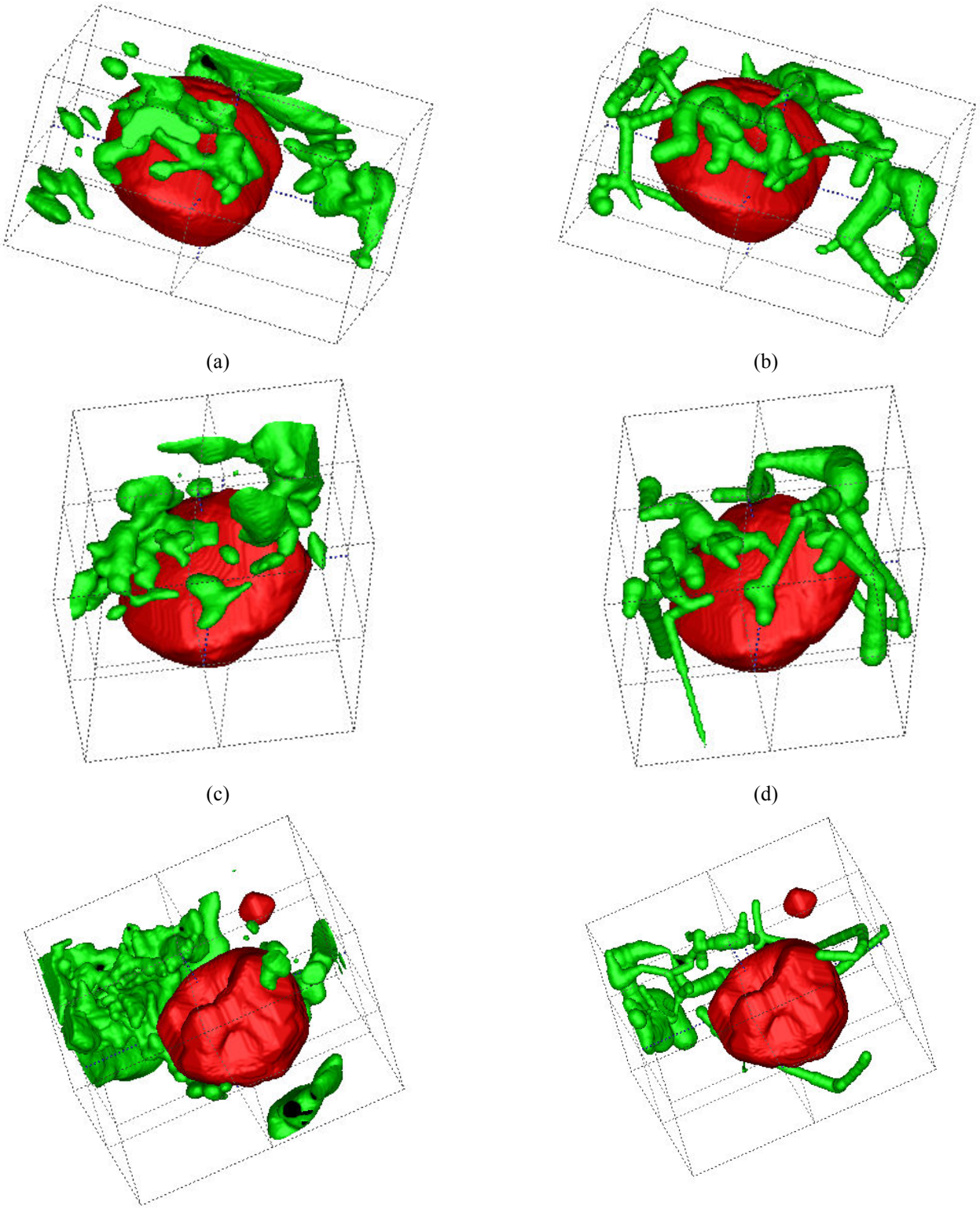

(a) (b) (c) (d) (e) (f)

Figure 14: Follicle and vessels from binarised power Doppler for images 1 (a), 2 (c) and 3 (e). Follicle and reconstructed vessels for images 1 (b), 2 (d) and 3 (f). Images 1 and 2 belong to the same patient.